IOPscience iopscience.iop.org

Home Search Collections Journals About Contact us My IOPscience

Sites of Fe^{3+} impurities in a congruent $LiTaO_3$ crystal

This article has been downloaded from IOPscience. Please scroll down to see the full text article.

1989 J. Phys.: Condens. Matter 1 3591

(http://iopscience.iop.org/0953-8984/1/23/004)

View the table of contents for this issue, or go to the journal homepage for more

Download details:
IP Address: 171.66.16.93
The article was downloaded on 10/05/2010 at 18:16

Please note that terms and conditions apply.

J. Phys.: Condens. Matter 1 (1989) 3591–3600. Printed in the UK

Sites of Fe^{3+} impurities in a congruent $LiTaO_3$ crystal

H Söthe†, L G Rowan‡ and J-M Spaeth†

† University of Paderborn, Fachbereich Physik, Warburger Strasse 100A, D-4790 Paderborn, Federal Republic of Germany

‡ University of North Carolina, Department of Physics and Astronomy, Chapel Hill, NC 27514, USA

Received 1 November 1988

Abstract. With electron nuclear double resonance (ENDOR) the superhyperfine (SHF) interactions of Fe^{3+} impurities with five shells of Li neighbours were measured in a congruent $LiTaO_3$ crystal. From the analysis of the ENDOR spectra it is found that Fe^{3+} is on a substitutional Li^+ site on the threefold symmetry axis of the crystal. From the shape of the ENDOR spectrum it is concluded that most Fe^{3+} impurities are on very perturbed sites.

1. Introduction

$LiNbO_3$ and $LiTaO_3$ are dielectric crystals that are of particular interest because of the photo-refractive effects observed in these materials. The photo-refractive effect, which can be used for the storage of volume phase holograms, seems to be correlated to the presence of defects such as transition metal impurities (Lines and Glass 1977, Kurz *et al* 1977, Krätzig and Orlowski 1978). For an understanding of the role of impurities in the photo-refractive effect on a microscopic scale, it is necessary to know the location of those impurities in the lattice. The largest influence on the photo-refractive effect is reported for iron (Kurz *et al* 1977). In spite of many efforts both by optical and electron spin resonance (ESR) spectroscopy (Mehran and Scott 1972, Pechenyl 1984, Grachev and Malovichko 1985) as well as theory (Agulló-López and Müller 1987) to determine the site of Fe^{3+} in $LiNbO_3$, no safe conclusion could be drawn. A Li^+ substitutional site with C_3 symmetry is also discussed as a substitutional Nb^{5+} site, which seems to be favoured from the analysis of Mössbauer spectra (Keune *et al* 1976).

The site of a paramagnetic impurity could in principle be determined by electron nuclear double resonance (ENDOR) by resolving the superhyperfine (SHF) interactions between the magnetic moments of the unpaired electrons and the magnetic moments of the lattice nuclei. All attempts to do so in congruent $LiNbO_3:Fe^{3+}$ have so far failed. However, in $LiTaO_3:Fe^{3+}$ ENDOR experiments were successful. In this paper we report ESR and ENDOR investigations of Fe^{3+} impurities in $LiTaO_3$. It is shown that only a fraction of the Fe^{3+} impurities is located at a well defined lattice site, which is the substitutional Li site with C_3 symmetry.

2. Experimental

The $LiTaO_3$ crystal was doped with 0.01 at.% Fe and grown in air as a congruent crystal by Union Carbide. It is supposed to have a Li deficit. The crystal (provided by Professor

0953-8984/89/233591 + 10 $02.50 © 1989 IOP Publishing Ltd

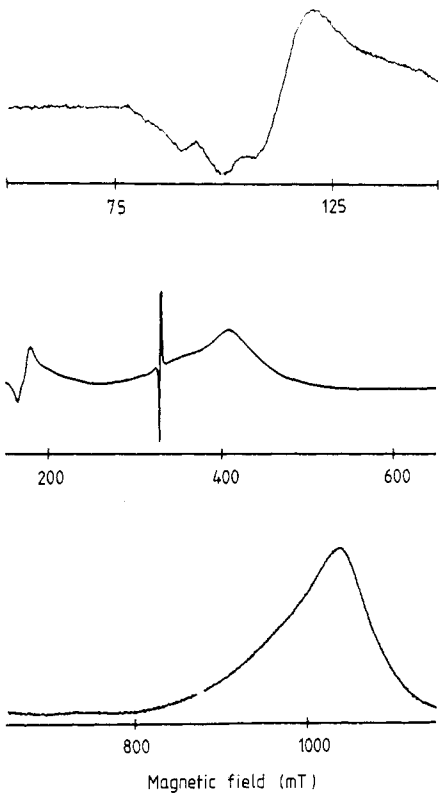

Figure 1. ESR spectrum of a congruent $LiTaO_3$ single crystal doped with Fe^{3+}. $T = 15$ K, $\nu_{ESR} = 9.2$ GHz, B_0 is perpendicular to the c-axis.

E Krätzig, University of Osnabrück) was oxidised to 90% in order to convert the Fe content into Fe^{3+}. Some measurements were also performed on congruent $LiNbO_3$ crystals doped with Fe^{3+} at several levels from a number of different suppliers.

The ESR and stationary ENDOR experiments were performed with a custom built computer-controlled X-band spectrometer. The sample temperature could be varied between 4 and 300 K, and the ENDOR frequency could be varied in the range between 0.5 and 80 MHz. The ENDOR spectra were digitally filtered. The ENDOR line positions were determined by using deconvolution algorithms and a special peak search algorithm (Niklas 1983).

3. Experimental results

3.1. Electron spin resonance

Figure 1 shows the ESR spectrum for the magnetic field $\boldsymbol{B}_0$ perpendicular to the c-axis of the crystal. The ESR lines at approximately 110 mT, 400 mT, and 1050 mT belong to the Fe^{3+} impurity. The sharp line at 330 mT is due to a DPPH field marker and the other lines at low field below 110 mT and at 180 mT are of unknown origin. The ESR spectrum was analysed with an axially symmetric spin Hamiltonian for the $3d^5$ ($S = 5/2$, $^6S_{5/2}$) configuration including the major crystal field term (Abragam and Bleaney 1970). The axial symmetry axis z is parallel to the c-axis of the crystal (see § 4):

$$H = \beta_e \boldsymbol{B}\tilde{\mathbf{g}}S + 3B_2^0(\mathbf{S}_z^2 - \tfrac{35}{12}). \tag{1}$$

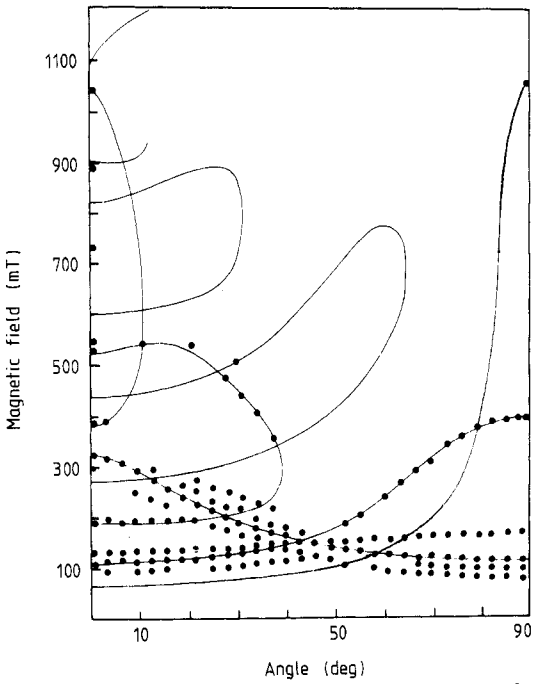

Figure 2. Angular dependence of the ESR spectrum of Fe^{3+} impurities in $LiTaO_3$ for rotation of the magnetic field from a parallel (0°) to perpendicular (90°) orientation with respect to the c-axis of the crystal. $T = 15$ K, $\nu_{ESR} = 9.2$ GHz.

The first term describes the electron Zeeman interaction, $3B_2^0$ is the crystal field parameter, and the other symbols have their usual meanings. The crystal field energy is of the same order as the electron Zeeman energy. Therefore, equation (1) had to be diagonalised numerically. In a high-field situation for a dominating electron Zeeman term one would expect five ESR transitions for $S = \frac{5}{2}$. In X-band (9.2 GHz) only the three transitions at 110 mT, 400 mT and 1050 mT could be observed for the magnetic field B_0 perpendicular to the c-axis. The X-band microwave energy is not high enough to induce more transitions. A similar situation was also found for Fe^{3+} in $LiNbO_3$ where the crystal field term was also very large (Mehran and Scott 1972). The angular dependence for rotation of $\boldsymbol{B}_0$ from the orientation parallel to the c-axis to perpendicular to the c-axis (figure 2) has a complicated pattern because of the large crystal field effect. The solid lines were calculated with the diagonalisation of equation (1) and are in very good agreement with the experimental line positions of Fe^{3+} centres (dots). Mainly below 300 mT several weaker ESR lines were also measured, which are of unknown origin. The peak positions of the ESR lines can be explained with a practically isotropic g-value of $g = 1.995 \pm 0.002$ and $3B_2^0 = 9900 \pm 100$ MHz. Higher-order crystal field terms were neglected since they must be small (< a few % of $3B_2^0$). Because of the large line width and strange line shape (see figure 1), which is not understood in detail, it seemed infeasible to try to determine the small higher-order terms. Comparison with ESR results for Fe^{3+} in $LiNbO_3$ shows a similar angular dependence pattern, and unusual ESR line shapes were observed (Towner *et al* 1971).

3.2. Electron nuclear double resonance (ENDOR)

Stationary ENDOR spectra were measured by partially saturating the ESR transition at 400 mT for the magnetic field perpendicular to the c-axis. This ESR line is isotropic upon

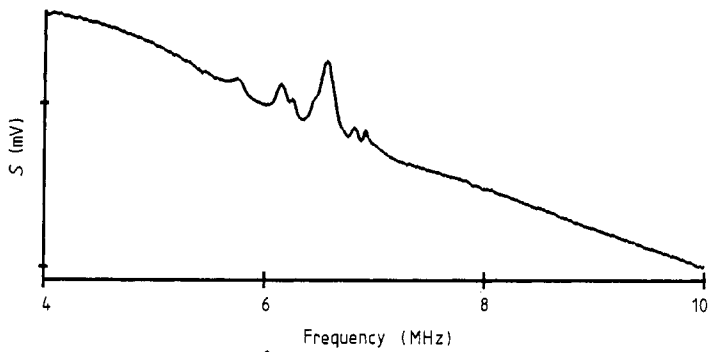

Figure 3. ENDOR effect of Fe^{3+} impurities above 4 MHz in $LiTaO_3$ when saturating the ESR transition at 400 mT. $T = 4.5$ K.

field rotation in the plane perpendicular to the *c*-axis. Figure 3 shows the ENDOR effect, i.e., the desaturation of the partially saturated ESR line (Seidel 1961), as a function of the radio frequency above 4 MHz inducing the nuclear magnetic resonance transitions. There is a rather large ENDOR effect in the 1.0–10 MHz frequency range, but only very small narrow lines are measured between 5 and 8 MHz. Above 10 MHz the ENDOR effect decreases rapidly. In all congruent $LiNbO_3$ crystals doped with Fe^{3+} we found only this broad desaturation effect up to approximately 10 MHz, but no sharp ENDOR lines. This broad ENDOR range does, however, belong to Fe^{3+} defects in both $LiTaO_3$ and $LiNbO_3$, as was seen from ENDOR-induced ESR measurements. In such an experiment the ENDOR effect can be measured by varying the magnetic field (field-swept ENDOR); one measures a kind of ESR excitation spectrum of the ENDOR lines (for details see Niklas and Spaeth 1980). The three ESR lines due to Fe^{3+} in figure 1 appear as ENDOR-induced ESR spectra when setting the radio frequency (RF) to the frequency of the narrow ENDOR lines of figure 3 and assuming that Li nuclei are responsible for them (see below; Niklas and Spaeth 1980). The ESR line shapes measured for Fe^{3+} in $LiTaO_3$ are reproduced very well. The Fe^{3+} ESR lines also appear, however, when setting the RF to anywhere in the broad ENDOR range. In $LiNbO_3$, where only the ENDOR range appears, the ENDOR-induced ESR spectra also reproduce the Fe^{3+} ESR lines. This unusual result indicates that in the ENDOR range there are many ENDOR lines with different frequencies superimposed such that only their envelope is measured. This could be the case if the local environment of the Fe^{3+} is not well defined (see § 4). For $B = 400$ mT the Larmor frequency of ^7Li is 6.6 MHz, for ^{181}Ta it is 2.1 MHz, and one would expect ENDOR lines around these two frequencies. Oxygen has no magnetic isotope with sufficient abundance to be observed. However, from the shape of the ENDOR range in figure 3 no quantitative conclusion can be drawn upon an ENDOR line distribution. On the one hand, the ENDOR line intensities are very poorly understood, the variation in the RF intensity is not precisely known within the frequency range, and at low frequencies the so-called $1/f$ (f = frequency) ENDOR desaturation effect plays a role that originates in RF field inhomogeneities in the sample, which is also only qualitatively understood (Seidel 1961). It is possible that other effects also contribute to the desaturation in this ferroelectric crystal, but at present these are not understood.

Figure 4 shows the spectrum of the sharp ENDOR lines after subtraction of the smooth envelope signal discussed above. Several clear ENDOR lines are measured around the ^7Li Larmor frequency. The spin Hamiltonian describing the ENDOR transitions including SHF interactions is:

$$H = \beta_e \boldsymbol{B}\tilde{\mathbf{g}}\boldsymbol{S} + 3B_2^0(S_z^2 - \tfrac{35}{12}) + \sum_{i=1}^{N} (\boldsymbol{S}\tilde{\mathbf{A}}_i\boldsymbol{I}_i - g_{\mathrm{I},i}\beta_n \boldsymbol{I}_i \cdot \boldsymbol{B}). \tag{2}$$

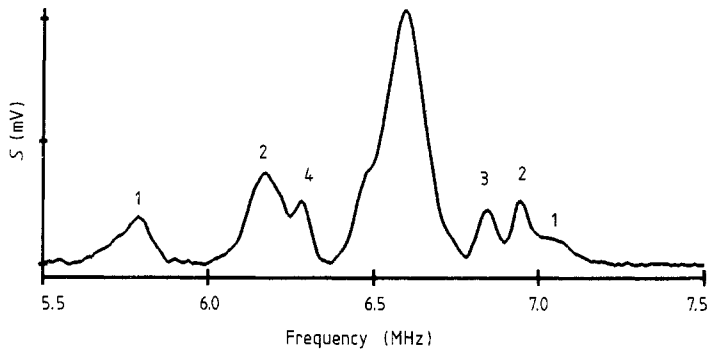

Figure 4. ENDOR lines of Fe^{3+} impurities in $LiTaO_3$ after subtraction of the smooth background signal of figure 3. The numbers denote the identified ^7Li shells. B_0 is perpendicular to the c-axis and parallel to the y-axis (see figure 7).

$\tilde{\mathbf{A}}_i$ is the SHF tensor of a lattice nucleus. The sum runs over all lattice nuclei which have SHF interactions. $g_{I,i}$ is their nuclear g-factor. Quadrupole interactions were neglected, since they could not be detected in the ENDOR spectra. In order to calculate the ENDOR frequencies, equation (2) can be diagonalised with sufficient accuracy in two steps. First, the electron Zeeman and the crystal field term were diagonalised numerically and an effective spin quantum number m_{seff} was calculated as $\langle S_z \rangle = m_{seff}$. Its value depends on B_2^0 and the magnetic field B_0 where the ENDOR transition was measured. This m_{seff} is then introduced in the nuclear spin Hamiltonian (the third term of equation (2)), which is then diagonalised within the nuclear quantum states.

For the ENDOR frequencies of each nucleus i one obtains:

$$\nu_i = (1/h)|m_{seff}(B_0, B_2^0)A_i(\theta_i, \varphi_i, \psi_i) - g_{I,i}\beta_n B_0| \tag{3}$$

where $A_i(\theta_i, \varphi_i, \psi_i)$ is the SHF interaction energy and depends on the SHF tensor orientation of neighbouring nuclei relative to the defect centre. β_n is the nuclear magneton.

For $B_0 = 400$ mT, and for that B_2^0 value which describes the ESR according to equation (1), we obtained $m_{seff} = 1.61$ and $m_{seff} = 0.11$. The ESR transition occurs between the two states, which are characterised by these two m_{seff} values. If one interprets the large ESR line width as arising because of an inhomogeneous distribution of crystal field parameters B_2^0, then one can calculate m_{seff} as a function of B_0 and B_2^0 for the ESR line around 400 mT. The range of $3B_2^0$ obtained is between 8000 and 11 000 MHz. This range also approximately describes the width of the other two ESR transitions. It is found that the higher m_{seff} value varies by less than 1% through the ESR line width and can be taken as a constant in equation (3) for this ESR transition. The lower m_{seff} value varies by about 50% on varying the magnetic field through the ESR line. Figure 5 shows the variation of the ENDOR frequency for one ENDOR line when sweeping the magnetic field B_0 through the ESR line at 400 mT from 370 to 430 mT. The ENDOR line frequency varies linearly with B_0 within an experimental accuracy of ± 10 kHz for the line position with a slope given by $(1/h)\, g_I\beta_n$ for ^7Li. This shows that the ENDOR line comes from the interaction with a ^7Li nucleus and that m_{seff} is practically constant, as expected for $m_{seff} = 1.61$. All measured ENDOR lines show this linear field shift behaviour. We have seen ENDOR transitions arising only from the $m_{seff} = 1.61$ quantum state. Had we also seen ENDOR lines belonging to the $m_{seff} = 0.11$ quantum state, then their frequency variation with B_0 through the ESR line should have followed the dashed line in figure 5. This was not

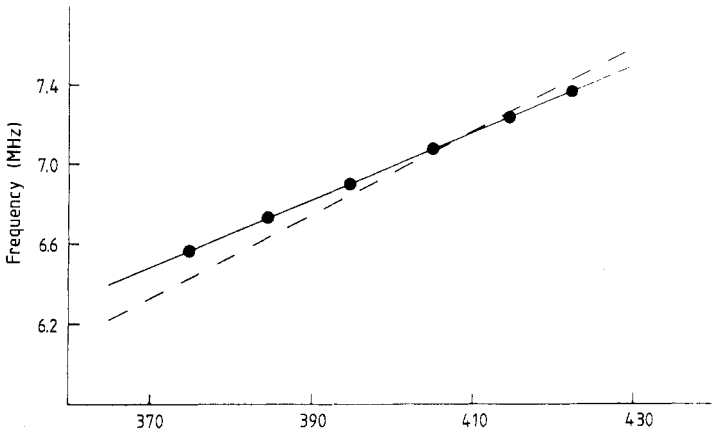

Figure 5. ENDOR frequency shift as a function of the magnetic field when measured through the 400 mT ESR line. The dashed line is expected for $m_{seff} = 0.11$, the solid line for $m_{seff} = 1.61$. The dots represent the experimental data.

observed. No narrow Ta ENDOR lines could be measured.

Figure 6 shows the ENDOR line angular dependence measured at 4.5 K for rotation of the magnetic field in a plane perpendicular to the *c*-axis. The experimental line positions are shown as dots. What is seen immediately is a 60° symmetry of the line patterns, which indicates that Fe^{3+} must be on the C_3 symmetry axis of the crystal, which is in accordance with the isotropic nature of the ESR line in that plane. There are two likely substitutional sites for Fe^{3+}: a substitutional Li^+ or a substitutional Ta^{5+} site. These two sites are schematically depicted in figures 7 and 8, in which only the Li lattice nuclei and the Ta nuclei on the *c*-axis are drawn for the sake of clarity (oxygens could not be observed). In the ferroelectric phase the *c*-axis is a threefold symmetry axis. There is also a mirror symmetry about three planes that are 60° apart and intersect in the *z*-axis (Weis and Gaylord 1985).

Unfortunately, an ENDOR line angular dependence could not be measured for rotation of the magnetic field in a plane connecting the $\boldsymbol{B}_0 \| c$ and $\boldsymbol{B}_0 \perp c$ orientations. The ENDOR lines are all near the ^{7}Li Larmor frequency ν_K (^{7}Li), e.g., their SHF interactions are small. Since they cross the ν_K (^{7}Li) value it is also apparent that the isotropic SHF constants (Fermi contact terms) must be very small (Seidel 1966). The solid lines in figure 6 are the calculated angular dependences according to equation (3) assuming that the Fe^{3+} is located at a substitutional Li^+ site on the *c*-axis and that the SHF interaction is due to the classical point dipole–dipole interaction only. The angular ENDOR pattern is described rather well by this simple assumption. The different Li shells are numbered as is shown in figure 7. In table 1 the distances are listed between the Li shell nuclei and the Fe^{3+}_{Li}. The angular dependence for the classical point dipole–dipole interaction assuming a Ta^{5+} site for Fe^{3+} is shown in figure 9 as solid lines. There is no convincing resemblance to the experimental angular dependence (dots). In particular, for this site one should have observed one isotropic ENDOR line (first shell) with a large interaction, since the nearest Li neighbour (first shell; see table 1) is on the *c*-axis. A second isotropic line with an interaction about 1 MHz lower than that would have also been expected. The signal-to-noise ratio of the ENDOR lines was good enough to observe single nuclei. We conclude, therefore, that Fe^{3+} must be on a Li site. An excellent agreement between

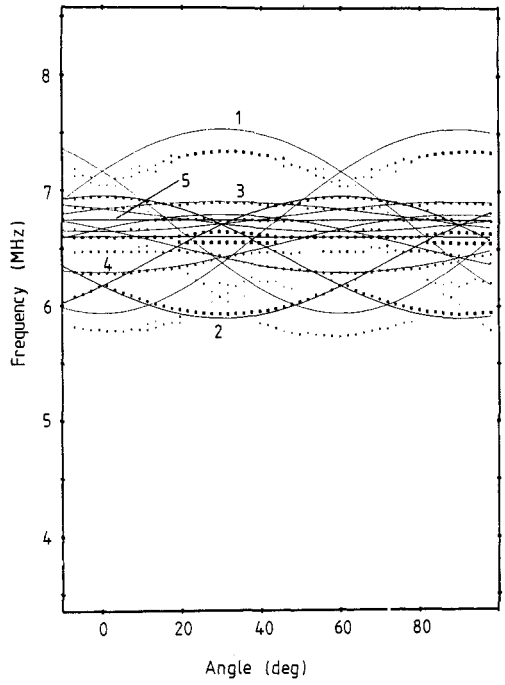

Figure 6. Angular dependence of the Li ENDOR spectrum for rotation of the magnetic field in a plane perpendicular to the c-axis. The dots are the experimental line positions. The solid lines represent the calculated angular dependence assuming that the SHF interaction is the classical point dipole–dipole interaction for Fe^{3+} occupying a substitutional Li^+ site. The numbers on the branches indicate the Li shells. 0° $\triangleq \boldsymbol{B}_0 \| y$-axis, 90° $\triangleq \boldsymbol{B}_0 \| x$-axis (see figure 7).

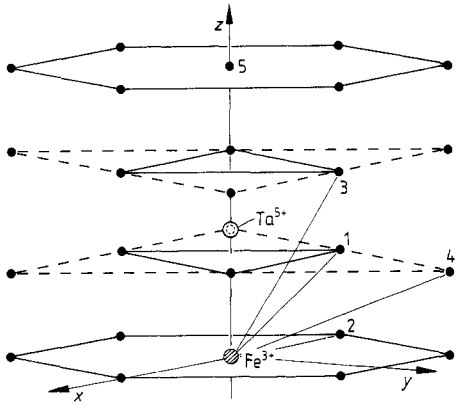

Figure 7. Schematic representation of the Li^+ subshell assuming Fe^{3+} to be on a substitutional Li site. The numbers 1–5 represent the Li shells with increasing distance from the Fe^{3+}. The Ta^{5+} position on the c-axis is also indicated (open circle).

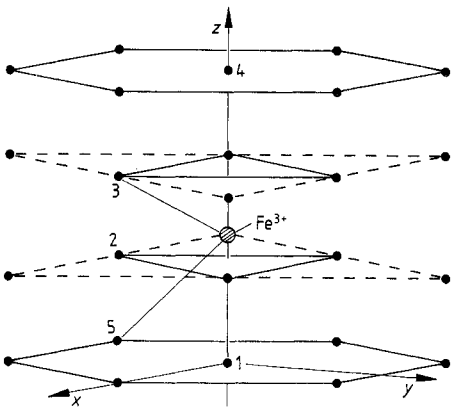

Figure 8. Schematic representation of the Li subshell assuming Fe^{3+} on a substitutional Ta^{5+} site. The numbers 1–5 represent the Li shells with increasing distance from the Fe^{3+}.

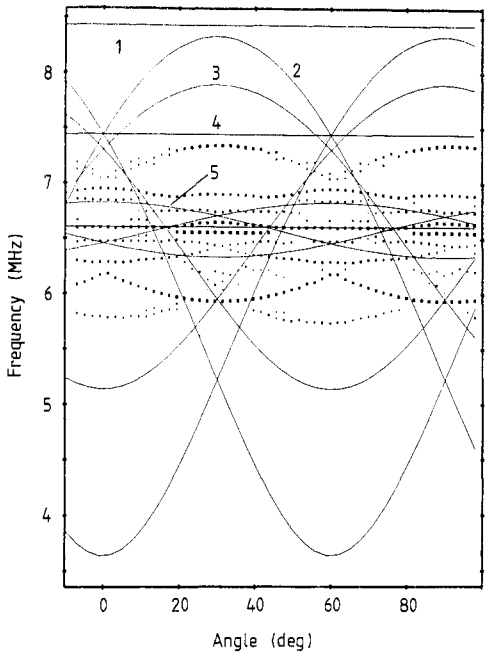

Figure 9. Angular dependence of the Li ENDOR spectrum for rotation of the magnetic field in a plane perpendicular to the *c*-axis. The dots are the experimental line positions. The solid lines represent the calculated ESR angular dependence for the assumption that the SHF interaction is the classical point dipole–dipole interaction for Fe^{3+} occupying a substitutional Ta^{5+} site. The numbers on branches indicate the Li shells (see figure 8).

Table 1. Distance between the nuclei of five Li neighbour shells from the Fe^{3+} impurity on a Li^+ site and a Ta^{5+} site (in Å) calculated from lattice parameters given in Abrahams and Bernstein (1967).

Li shell	Li^+ site	Ta^{5+} site
1	3.76	3.00
2	5.15	3.06
3	5.47	3.37
4	6.38	3.89
5	6.89	5.97

experimental and calculated angular dependence for the Li site is obtained for the SHF interaction parameters given in table 2 in terms of the isotropic SHF constants a and the anisotropic constants b. These constants are related to the principal values of the SHF tensor $\tilde{\mathbf{A}}$ by

$$a = \tfrac{1}{3}(A_{xx} + A_{yy} + A_{zz}) \qquad b = \tfrac{1}{2}(A_{zz} - a). \tag{4}$$

The excellent agreement is obtained by assuming that the z-axes of the SHF tensors are parallel to the connection lines between the shell nuclei and the Fe^{3+}_{Li}. This is expected

Table 2. Superhyperfine interactions of five Li shells surrounding Fe^{3+} impurities in $LiTaO_3$ and the classical point dipole–dipole SHF interaction constants b_{dd} calculated assuming that Fe^{3+} is on a substitutional Li^+ site (in MHz). The experimental uncertainty is ±0.015 MHz.

Shell	a	b	b_{dd}
1	0.118	0.58	0.58
2	−0.015	0.21	0.22
3		0.19	0.19
4		0.12	0.12
5		0.09	0.09

if the interaction is almost entirely the classical dipole–dipole interaction.

4. Discussion

The analysis of the ENDOR angular dependence clearly shows that the site of the Fe^{3+} must be a substitutional Li^+ site. The fact that we observed only very small isotropic interactions even for the nearest first-shell Li neighbours shows that the five 3d orbitals do have very little overlap transfer via the oxygen neighbours to the Li shells. Since the anisotropic SHF constants b are explained so well by the point dipole–dipole interaction for the regular lattice distances of the Li^+ shells from a substitutional Li^+ site, it is concluded that the site of Fe^{3+} is rather well defined with respect to the Li sublattice for those defects which gave rise to the narrow-line ENDOR spectrum.

The narrow ENDOR lines, however, are rather broad compared to what one finds for point defects in well defined ionic lattices, where a typical ENDOR line width is of the order of 10–20 kHz, while the lines here have approximately 70 kHz half-width (e.g., second shell; see figure 4). This indicates that the distances between Li neighbours and Fe^{3+} vary somewhat. On the basis of the dipole–dipole interaction an estimate for the second-shell Li neighbours yields that the Li^+–Fe^{3+} distance may vary by ±0.12 Å. This estimate is an upper limit, because it assumes that the line width is not caused by unresolved quadrupole interactions. The plane spanned by Fe^{3+} and the second-shell Li^+ is a mirror plane with respect to the Li sublattice. If Fe^{3+} was moved away from the Li site on the c-axis towards a Ta^{5+} site, one would have observed an ENDOR line splitting of the Li shells (except the second shell). This was not observed. An off-centre position must be small enough not to cause a line splitting, which limits it to be smaller than ±0.05 Å as estimated as an upper limit from the first-shell line shape.

The observation of the broad ENDOR range as smooth background signal indicates that probably most Fe^{3+} impurities are on sites that are locally rather poorly defined due to defects, probably due to many cation vacancies, which are expected because of charge compensation and due to an imperfect crystal composition. Apparently, the congruent $LiTaO_3$ was a better crystal than all the congruent $LiNbO_3$ crystals we tried to measure. A recent observation of narrow Li and Nb ENDOR lines in an almost stoichiometric $LiNbO_3$ crystal doped with Fe^{3+} supports this interpretation (Corradi *et al* 1989). The almost stoichiometric crystal must possess more well defined Fe^{3+} sites.

The largest Li frequency observed in the ENDOR range is about 10 MHz, which corresponds to a Fe^{3+}–Li^+ distance of between 2.5 and 3 Å, depending on the tensor orientation with respect to B_0. Such distances are expected if Fe^{3+} was displaced along the c-axis up to about the first-shell plane in figure 7. ^{181}Ta lines are expected around

2.1 MHz (ν_K ^{181}Ta for 400 mT). The lower-frequency part of the ENDOR range is probably due to small ^{181}Ta interactions.

5. Conclusions

Our experiments and analyses have shown that those Fe^{3+} ions in a congruent $LiTaO_3$ crystal, which are on well defined sites, occupy substitutional Li sites with an accuracy of better than approximately ± 0.1 Å as far as the distance to the nearby Li^+ sublattice is concerned. Most Fe^{3+} impurities occupy sites, with nearby defects that probably also cause Fe^{3+} displacement along the *c*-axis in such an irregular way, that narrow ENDOR lines can no longer be observed.

Acknowledgments

One of us (LGR) gratefully acknowledges the Deutsche Forschungsgemeinschaft for a grant to conduct experiments at the University of Paderborn.

References

Abragam A and Bleaney B 1970 *Electron Paramagnetic Resonance of Transition Ions* (Oxford: Clarendon)
Abrahams S C and Bernstein J L 1967 *J. Phys. Chem. Solids* **28** 1685
Agulló-López F and Müller K A 1987 *Cryst. Latt. Def. and Amorph. Mater.* **15** 89
Corradi G, Söthe H and Spaeth J M 1989 unpublished
Grachev V G and Malovichko G I 1985 *Sov. Phys. Solid State* **27** 424
Keune W, Date S K, Gonser U and Bunzel H 1976 *Ferroelectrics* **13** 443
Krätzig E and Orlowski R 1978 *Appl. Phys.* **15** 133
Kurz H, Krätzig E, Keune W, Engelmann H, Gonser U, Dischler B and Räuber A 1977 *Appl. Phys.* **12** 355
Lines M E and Glass A M 1977 *Principles and Applications of Ferroelectrics and Related Materials* (Oxford: Clarendon)
Mehran F and Scott B A 1972 *Solid State Commun.* **11** 15
Niklas J R 1983 *Habilitationsschrift* Paderborn
Niklas J R and Spaeth J M 1980 *Phys. Stat. Solidi* b **101** 221
Pechenyl A P 1985 *Sov. Phys.–Solid State* **27** 923
Seidel H 1961 *Z. Physik* **165** 218
—— 1966 *Habilitationsschrift* Stuttgart
Towner H H, Kim Y M and Story H S 1971 *J. Chem. Phys.* **56** 3676
Weis R S and Gaylord T K 1985 *Appl. Phys.* A **37** 191